

Tomography of time-bin quantum states using time-resolved detection

Karolina Sedziak-Kacprowicz, Artur Czerwinski, and Piotr Kolenderski*

Faculty of Physics, Astronomy and Informatics, Nicolaus Copernicus University, Grudziadzka 5, 87-100 Toruń, Poland

(Dated: July 2, 2022)

We present a method for measuring quantum states encoded in temporal modes of photons. The basis for the multilevel quantum states is defined based on modes propagating in a dispersive medium, which is a fiber in this case. The propagation and time-resolved single photon detection allows us to define a positive-operator valued measurement (POVM). The POVM depends on the amount of dispersion and the characteristics of a detector. This framework is numerically tested by performing quantum state tomography on a large number of states for a set of realistic experimental settings. Finally, the average fidelity between the expected and reconstructed states for qubits and qutrits is computed.

I. INTRODUCTION

Quantum communication protocols can be implemented using photonic states. A generic scheme is based on transmission of a single photon through a channel to a receiver. Information can be encoded, for example in polarization [1], spatial [2, 3] or spectral modes [4]. The channel properties and the receiver characteristics determine the optimal protocol assuring the best performance. Free space [5–7] and fiber-based [8] quantum communication links have been demonstrated. Each of them has its advantages and disadvantages. Both suffer from several effects limiting their maximal distance and throughput. Typical fiber introduces uncontrollable polarization transformation, which must be taken into account [9], when a qubit is encoded in polarization. Fiber links are also subjected to dispersion and loss, which, when combined with imperfect detectors, limit the transmission maximal range [10]. On the other hand, one can take advantage of the propagation effects in the fiber to extend the distance of quantum communication protocols [11], when time-resolved single photon detection is available.

It is also possible to encode information in the temporal domain by using interferometric techniques. The first proposal involving time-bin encoding was introduced by Franson in the context of the violation of Bell inequalities [12]. This idea was also applied for quantum key distribution [13] protocols and more recently for quantum information processing [14, 15]. This experimental technique requires one unbalanced interferometer to prepare time-bin states and another interferometer or a nonlinear interaction for measurement. The advantages are the noise robustness during propagation of photons and a simplified experimental setup to realize quantum communication protocol.

We present a framework where the Hilbert space of a multilevel system, a qudit, can be established based on a discrete number of separated temporal modes of a single photon. This is in the time-bin encoding framework [12]. The unitary evolution that the photon experiences during

propagation in a dispersive medium can be interpreted as an evolution of a qudit state within Schrödinger picture. On the other hand, the Heisenberg representation allows us to define measurement operators which change in time. In this paper we first introduce the framework for qubits and generalize it for qudits. Next, the method's robustness is tested numerically by analysing the quantum state tomography results for qubits and qutrits. This is analogous to spatial encoding in the transverse momentum of a photon [16], where the photon propagates through a system of multiple slits that defines its state. The photon is then measured using spatially-resolved single photon detection technique, which defines a POVM.

II. TEMPORAL ENCODING

A. Qubit

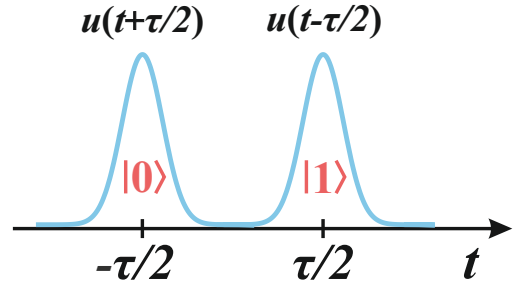


FIG. 1. A single qubit is defined as a photon which is delocalised in two wave packets separated in time interval $[-\tau/2, \tau/2]$.

Let us assume a physical situation where a single photon state is described by a wave function that is the sum of a pair of separated temporal modes:

$$\psi(t) = \alpha_0 u(t + \tau/2) + \alpha_1 u(t - \tau/2), \quad (1)$$

where α_0 and α_1 are complex numbers satisfying the nor-

* kolenderski@fizyka.umk.pl

malization condition, $|\alpha_0|^2 + |\alpha_1|^2 = 1$, and

$$u(t) = \frac{e^{-\frac{t^2}{2\sigma^2}}}{\sqrt{\sqrt{\pi}\sqrt{\sigma}}}. \quad (2)$$

This is depicted in Fig. 1. Let us now define the following vectors:

$$|0\rangle = \int dt u(t + \tau/2) |t\rangle \quad (3)$$

$$|1\rangle = \int dt u(t - \tau/2) |t\rangle, \quad (4)$$

where $|t\rangle$ represents the state of a photon localized within a time instant t . The overlap of the two state vectors reads:

$$\langle 0|1\rangle = e^{\frac{-\tau^2}{4\sigma^2}}, \quad (5)$$

which means that they are not perfectly orthogonal but can be made approximately so by a proper choice of the ratio of the modes' separation, τ , to their widths σ . A realistic assumption is $\langle 0|1\rangle = 3 \times 10^{-7}$ for $\tau/\sigma = 7.7$. Therefore, we can consider $\{|0\rangle, |1\rangle\}$ as an orthogonal basis. This allows us to define a logic qubit state as:

$$|\psi_{in}\rangle = \alpha_0 |0\rangle + \alpha_1 |1\rangle. \quad (6)$$

It is the definition that will be generalized in the next section. To define the measurements on a logic qubit, let us first consider a wave packet, $u_L(t)$, propagated through a fiber characterized by length L and dispersion parameter β . This can be modelled as an action of a propagator, $\mathcal{S}(t, t', L)$, on an initial state, $u(t')$, in the following way [10]:

$$u_L(t) = \int dt' \mathcal{S}(t, t', L) u(t'). \quad (7)$$

For the propagator related to a dispersive fiber (see Ref. [10] for details) this results in:

$$u_L(t) = \frac{e^{\frac{it^2}{4\beta L - 2i\sigma^2}}}{\sqrt[4]{\pi}\sqrt{\sigma + \frac{2i\beta L}{\sigma}}}. \quad (8)$$

With this result, we can apply Born's rule to compute the probability density of detecting a photon at time, t after the propagation:

$$p(t) = |\alpha_0 u_L(t + \tau/2) + \alpha_1 u_L(t - \tau/2)|^2. \quad (9)$$

We observe that the last equation can be rewritten as:

$$p(t) = \text{Tr} \left(\hat{M}(t) |\psi_{in}\rangle \langle \psi_{in}| \right). \quad (10)$$

Here the measurement operator is given by:

$$\hat{M}(t) = \mu(t) |\psi_M(t)\rangle \langle \psi_M(t)|. \quad (11)$$

with

$$\mu(t) = \frac{\sigma}{\sqrt{\pi}\sqrt{4\beta^2 L^2 + \sigma^4}} \left(e^{-\frac{\sigma^2(t+\tau/2)^2}{4\beta^2 L^2 + \sigma^4}} + e^{-\frac{\sigma^2(t-\tau/2)^2}{4\beta^2 L^2 + \sigma^4}} \right), \quad (12)$$

interpreted as the weight of the normalized state defined as:

$$|\psi_M(t)\rangle = \frac{1}{\sqrt{\mu(t)}} \begin{pmatrix} u_L(t + \tau/2) \\ u_L(t - \tau/2) \end{pmatrix}. \quad (13)$$

Note that operator, $M(t)$, depends only on the fiber parameters L and β and does not depend on the initial state $|\psi\rangle$. It can also be easily shown that it obeys the following relation:

$$\int \hat{M}(t) dt = \begin{pmatrix} 1 & e^{-\tau^2/4\sigma^2} \\ e^{-\tau^2/4\sigma^2} & 1 \end{pmatrix} \approx \mathbb{1}, \quad (14)$$

which makes it a proper POVM with the approximation that the off-diagonal terms are negligible. The same assumptions make the basis states orthogonal.

The POVM set can be visualized using the Bloch sphere to represent a state $|\psi_M(t)\rangle$ as a point and the measurement weight, $\mu(t)$, by assigning a color to the point using a temperature scaling. An example for a typical telecom fiber (SMF28e+) can be seen in the first row in Fig. 2. The fiber and wave packet parameters are the following: $\beta = -1.15 \times 10^{-26} \frac{s^2}{m}$, $\sigma = 0.65$ ps and $\tau = 5$ ps throughout the paper. The points corresponding to the measurement time instances form a spiral on the Bloch sphere. The plot shows a discrete set of time instances for which the POVM probability, $\mu(t)$, is greater than 5 %. The spiral is more squashed for longer fibers as seen by comparing the pictured POVM for fiber lengths $L = 200$ m and $L = 500$ m.

In the Fig. 2 under each Bloch sphere we simulated outcome of photon arrival time detection for different values of length of the link L and detector jitter σ_D for input state $\frac{1}{\sqrt{2}}(|0\rangle + |1\rangle)$.

In practice, single photon detection systems feature timing jitter, which is an uncertainty in the measured arrival time of the particle. A timing uncertainty of the detection process can be modelled by convoluting the real probability distribution, $p(t)$ given in Eq. 9, with a Gaussian distribution defined by:

$$q_D(t) = \frac{\exp\left(-\frac{t^2}{2\sigma_D^2}\right)}{\sqrt{2\pi\sigma_D^2}}, \quad (15)$$

where σ_D is the timing jitter. This parameter in the case of superconducting nanowire single-photon detectors (SNSPDs) is of the order of 25 ps [17, 18] and for state-of-the-art ones can reach 1 ps [19]. The POVM, when taking imperfect detectors into account can then be written as:

$$\hat{M}_D(t) = \int \hat{M}(t') * q_D(t - t') dt'. \quad (16)$$

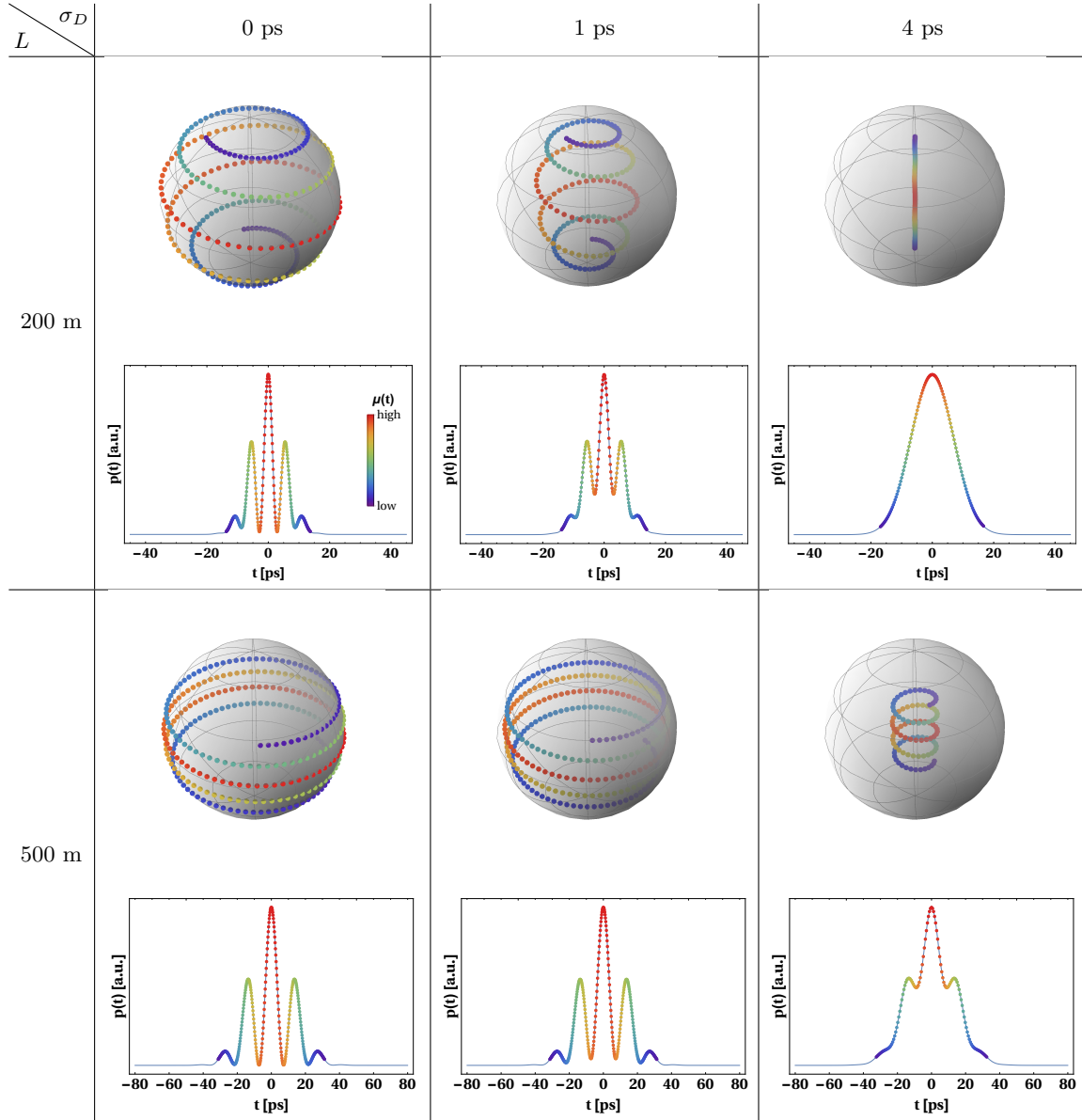


FIG. 2. Visualization of a POVM set on the Bloch sphere in an ideal scenario (first column) and in the cases of the detector jitter of 1 ps (second column) and 4 ps (third column). Under each Bloch sphere we put the probability density, $p(t)$, given by Eq. 9 after propagation through a fiber link by an example input state $\frac{1}{\sqrt{2}}(|0\rangle + |1\rangle)$. In the rows we put different values of the fiber length. The color in the temperature mapping represents the probability density of the measurement, $\mu(t)$ of the respective POVM element, where the most probable is colored with red (the highest $\mu(t)$).

The measurement operator $\hat{M}_D(t)$ can be decomposed in terms of mixed states as opposed to $\hat{M}(t)$, which is defined using pure states, see Eq. 11. This is illustrated in Fig. 2 where the second and third row show the impact of the detector imperfection. Even a very small jitter increases the entropy of the POVM significantly. Note that for 4 ps the spiral is degenerated to a line. This effect, however, can be partially compensated for by adding more dispersion (increasing the length of the fiber) as can be seen by comparing the POVMs in the last column. The larger standard deviation of the detector timing jitter makes the measurement points collapse

on the Bloch sphere, reducing the purity of the POVM state. The longer fiber results in measurement points that are localized near the equator. This means that one would be able to estimate only the phase of the entire state.

B. Qudit

The framework introduced for qubits can be easily generalized to qudits. We define a qudit as a photon delocalised in d wave packets separated by a time τ . A wave

function for a qudit can be defined, in analogy to Eq. 1, as:

$$\psi(t) = \sum_{n=0}^{d-1} \alpha_n u \left(t - n\tau + \frac{d-1}{2}\tau \right), \quad (17)$$

where α_n are complex numbers satisfying the normalization condition, $\sum_{n=0}^d |\alpha_n|^2 = 1$, and $u(t)$ is given by the Eq. 2. The basis vectors are defined by the following formula

$$|n\rangle = \int dt u \left(t - n\tau + \frac{d-1}{2}\tau \right) |t\rangle, \quad (18)$$

where $n = 0, \dots, d-1$, and $|t\rangle$ represents a d -dimensional state of a photon localized in time t . The overlap of two arbitrary states reads:

$$\langle n|k\rangle = e^{-\frac{\tau^2(k-n)^2}{16\sigma^2}}. \quad (19)$$

In turn the measurement operator as defined by Eq. 11 can be generalized by using weight:

$$\mu(t) = \frac{\sigma}{\sqrt{\pi}\sqrt{C}} \left(e^{-\frac{\sigma^2(t+\frac{d-1}{2}\tau)^2}{C^2}} + \dots + e^{-\frac{\sigma^2(t-\frac{d-1}{2}\tau)^2}{C^2}} \right), \quad (20)$$

and measurement vector

$$|\psi_M(t)\rangle = \frac{1}{\sqrt{\mu(t)}} \begin{pmatrix} u_L(t + \frac{d-1}{2}\tau) \\ u_L(t + \frac{d-3}{2}\tau) \\ \vdots \\ u_L(t - \frac{d-3}{2}\tau) \\ u_L(t - \frac{d-1}{2}\tau) \end{pmatrix}. \quad (21)$$

It can be shown that the completeness of the measurement operators also holds with the same assumption that the orthogonality of the basis states $\int \hat{M}(t)dt \approx \mathbb{1}$. Next, the detector jitter can be taken into account in the same way as before, Eq. 16. Similarly as for qubits, but only for the case with no detector jitter, the POVM can be represented on a Bloch ball by using Majorana representation [20, 21]. An example will be shown in the next section for a qutrit.

III. QUANTUM STATE TOMOGRAPHY

The measurement operators that were discussed in the previous section constitute an approximate POVM and can be used as a source of information for quantum state tomography. From an experimental point of view, it is not possible to obtain a perfect informationally-complete set of measurement operators. Therefore, we need to evaluate the efficiency of realistic measurement operators. We assume that a large number of identical copies of a given state are generated. The state is then reconstructed based on the statistics of the temporal detections, see example of $p(t)$ in Fig. 2. Mathematically, we

follow the Born rule given by Eq. 10 to describe the results of the measurement. In order to perform quantum state tomography, we assume that we are able to describe the imperfections of the detection system and therefore, we apply the formula for the detection probability which contains the detector jitter. However, the measurement results are burdened with the Poissonian noise which is a basic form of uncertainty associated with the measurement of photons. We take 26 measurement operators and each result is simulated assuming that there are 10^3 photons. This approach allows us to numerically generate a set of realistic data.

Then we employ two very widely used quantum tomography techniques: the maximum likelihood estimation (MLE) [22, 23] and the least squares (LS) method [24]. For the convenience of numerical analyses we adopt from [25] the parametrization of the unknown density matrix, which provides hermiticity, positivity and normalization:

$$\rho = \frac{T^\dagger T}{Tr\{T^\dagger T\}}, \quad (22)$$

where T denotes a complex triangular matrix. This parametrization ensures that the estimated matrix is physical and belongs to the quantum state set. The quality of the reconstructed state is quantified by computing the fidelity [26] between the initial and the estimated state. The fidelity is defined for two mixed quantum states ρ, σ by

$$\mathcal{F}(\rho, \sigma) := \left(Tr\sqrt{\sqrt{\rho}\sigma\sqrt{\rho}} \right)^2. \quad (23)$$

It is easy to verify that $0 \leq \mathcal{F}(\rho, \sigma) \leq 1$ and $\mathcal{F}(\rho, \sigma) = 1$ if and only if $\rho = \sigma$. Furthermore, it is symmetric, i.e. $\mathcal{F}(\rho, \sigma) = \mathcal{F}(\sigma, \rho)$, which does not stem straightforwardly from the definition. The formula Eq. 23 can be simplified if one considers only pure states, i.e. $\mathcal{F}(\rho, \sigma) = |\langle \psi_\rho | \psi_\sigma \rangle|^2$ for $\rho = |\psi_\rho\rangle \langle \psi_\rho|$ and $\sigma = |\psi_\sigma\rangle \langle \psi_\sigma|$.

The Poissonian noise is typical for measurements based on photon counting, which is the case for our application. We use quantum state fidelity $\mathcal{F}(\rho_{in}, \rho_{out})$ to evaluate the quality of our tomography framework. Since the value of this fidelity depends on the initial density matrix ρ_{in} , we introduce the *average fidelity*, \mathcal{F}_{av} as a figure of merit. It is defined as the mean value computed over all possible input state sets, ρ_{in} . It allows us to determine the average performance of our quantum tomography scheme. In practice, we cannot find analytically the average fidelity over the entire state set, so we select a representative sample of quantum states for numerical analysis. Then, each state from the discrete set is sent through the fiber and reconstructed based on the measurement results distorted by the Poissonian noise. The average fidelity for the finite sample can be used to estimate the effectiveness of our POVM in quantum state reconstruction.

A. Qubit

For a qubit, the triangular matrix, T , parametrizing the density operator, ρ , given by Eq. 22 takes the following form:

$$T = \begin{pmatrix} t_1 & 0 \\ t_3 + it_4 & t_2 \end{pmatrix}, \quad (24)$$

where $t_1, t_2, t_3, t_4 \in \mathbb{R}$. Thus, the problem of reconstructing the initial density matrix can be formulated in terms of determining the values of t_1, t_2, t_3, t_4 .

Numerical simulation has been conducted to test the effectiveness of our measurement operators for quantum tomography in different experimental setups. The main results are gathered in Tab. I. One can observe that for $\sigma_D = 0$ (measurements without jitter) both quantum tomography methods result in an average fidelity very close to 1. This outcome confirms that in the ideal scenario (no jitter) any quantum state can be reconstructed flawlessly and the Poissonian noise does not reduce the average fidelity. Both MLE and LS methods lead, on average, to the relevant quantum state.

If we analyze the results in the rows of Tab. I, one can easily notice that for a fiber length of 200 m the average fidelity decreases as the detector jitter increases. It is a consequence of the detector jitter leading to a greater uncertainty. However, when the detector jitter equals 1 ps, which is achievable in practice[19], both quantum tomography methods can still reconstruct the initial state with high accuracy.

The most interesting conclusion can be drawn if we compare the results in the columns. One can see that when the detector jitter is fixed at 4 ps, we obtain higher average fidelity for the longer fiber. In the case of $L = 200$ m the state reconstruction appears highly inaccurate since we have low average fidelity. However it can be improved if we extend the length of the fiber to 500 m. This means that the two parameters, the length of a fiber and the detector jitter, have opposing impacts on the average fidelity. One can reduce the errors due to the detector jitter by using a longer fiber. Numerical results are in agreement with Fig. 2, where the measurement points are depicted on the Bloch ball. For the fixed jitter the states generating the POVM are less mixed if the fiber is longer.

B. Qutrit

The basis states for a qutrit are defined as in Eq. 18 and the states generating the POVM are given by Eq. 21 for $n = 3$. To visualize the POVM on the Bloch sphere for qutrits we utilize Majorana representation [20]. It allows to associate a pair of two-dimensional states with a qutrit. For the qutrit measurement vector, given by Eq. 21, one can write a quadratic Majorana polynomial

L	σ_D	0 ps	1 ps	4 ps
200 m	LS	0.9995(12)	0.9982(18)	0.61(18)
	MLE	0.998(2)	0.987(11)	0.58(18)
500 m	LS	0.996(4)	0.9962(34)	0.9951(45)
	MLE	0.9921(31)	0.9897(42)	0.91(4)

TABLE I. Average fidelity with standard deviation for quantum tomography of qubits computed numerically for different values of experimental parameters. The results were obtained over a sample of 9261 qubits. The experimental results were simulated with the Poissonian noise. The same set of data was used for both LS and MLE quantum tomography techniques.

$$p(|\psi_M\rangle) = 0 [21]:$$

$$e^{\frac{i(t-\tau)^2}{4\beta L-2i\sigma^2}} z^2 - \sqrt{2} e^{\frac{it^2}{4\beta L-2i\sigma^2}} z + e^{\frac{i(t+\tau)^2}{4\beta L-2i\sigma^2}} = 0. \quad (25)$$

Stereographic projection is used to associate the two complex numbers with two points on the Bloch sphere. We visualize this for two different lengths of the fiber in order to see how pairs of points are distributed on the Bloch sphere.

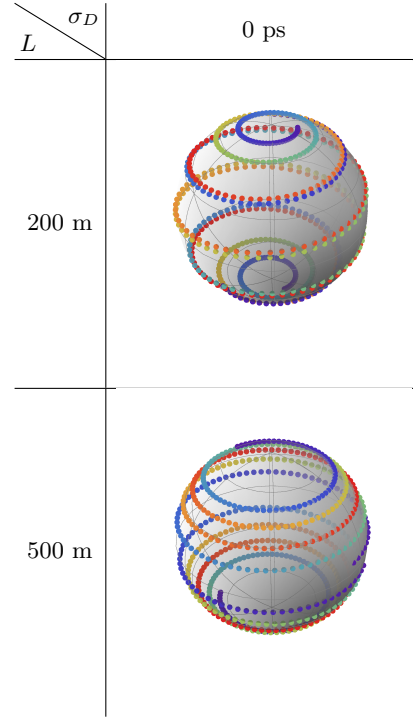


FIG. 3. Illustration of pairs of measurements points on the Bloch sphere for qutrits in the ideal scenario. In the columns we put different values of length of the fiber. The highest probabilities of our detector registering a photon are marked as red and the lowest probabilities in violet.

In the case of qutrits we follow a very similar quantum tomography procedure as for qubits. First, we use the same parametric-dependent formula for the unknown density matrix given by Eq. 22. Here, the matrix T de-

pends on 9 real parameters:

$$T = \begin{pmatrix} t_1 & 0 & 0 \\ t_4 + it_5 & t_2 & 0 \\ t_8 + it_9 & t_6 + it_7 & t_3 \end{pmatrix}. \quad (26)$$

Thus, the problem of state reconstruction for qutrits can be translated into finding the values of t_1, t_2, \dots, t_9 . Next, to evaluate the effectiveness of the POVM for qutrits, we follow exactly the same steps as for qubit.

L	σ_D	0 ps	1 ps	4 ps
		LS	0.988(13)	0.949(52)
200 m	MLE	0.79(16)	0.68(18)	0.58(25)
	LS	0.971(31)	0.969(31)	0.91(8)
500 m	MLE	0.80(16)	0.80(16)	0.68(17)
	LS			

TABLE II. Average fidelity with standard deviation for quantum tomography of qutrits computed numerically for different values of experimental parameters. The results were obtained over a sample of 9261 qutrits. The experimental results were simulated with the Poissonian noise. The same set of data was used for both LS and MLE quantum tomography techniques.

The results of the average fidelity for quantum tomography of qutrits are gathered in Tab. II. One can observe that in the case of perfect measurements (no jitter), both methods can reconstruct the initial quantum state with only limited accuracy. Especially, the estimation based on the MLE leads to a significant error rate.

If we analyze the results in the row for $L = 200$ m, we can observe a substantial influence of the detector jitter on the average fidelity. Particularly, if $\sigma_D = 4$ ps the average fidelities are relatively small, but they are exactly the same as in case of qubit reconstruction. The difference is that for qutrits we get a higher standard deviation, which means that the variation of the set of average fidelities is greater than in case of qubits.

Two conclusions can be drawn from the results in the columns. First, if $\sigma_D = 1$ ps or $\sigma_D = 4$ ps, the MLE and LS methods appear to follow the same tendency as for qubits, i.e. the average fidelity increases when we use a longer fiber. Second, it should be noted that for $\sigma_D = 4$ ps the LS method results in a larger fidelity improvement for a longer fiber.

Finally, special attention should be given to the performance of the MLE. Whereas for qubits both quantum tomography methods lead to very similar results, in the case of qutrits the performance of the MLE is significantly worse than the LS method.

IV. SUMMARY AND OUTLOOK

In conclusion, we have demonstrated an effective method of measuring quantum states encoded in temporal modes of photons. Numerical tools allowed us to verify under which circumstances the reconstruction methods are most effective for a set of realistic experimental parameters. To investigate the performance of our quantum state tomography schemes, we employed the average fidelity. Our analysis indicates that a longer fiber can compensate for the effects caused by detector jitter.

There are a number of issues that need further investigation. For example, it remains unclear why the MLE method does not give the accurate reconstruction of qutrits. Moreover, it will be useful to perform more numerical simulations of the average fidelity for a wider range of parameters in order to obtain a broad view on the effectiveness of our schemes. This task requires more processing power and for this reason it will be the subject of future research.

FUNDING INFORMATION

Foundation for Polish Science (FNP) (project First Team co-financed by the European Union under the European Regional Development Fund); National Science Centre, Poland (NCN) (grant no. 2016/23/N/ST2/02133).

ACKNOWLEDGMENTS

The authors acknowledge support by the National Laboratory of Atomic, Molecular and Optical Physics, Torun, Poland.

[1] C. Clausen, F. Bussieres, A. Tiranov, H. Herrmann, C. Silberhorn, W. Sohler, M. Afzelius, and N. Gisin, *New J. Phys.* **16**, 093058 (2014).

[2] G. Lima, A. Vargas, L. Neves, R. Guzmán, and C. Saavedra, *Opt. Express* **17**, 10688 (2009).

[3] M. A. Solís-Prosser, A. Arias, J. J. M. Varga, L. Rebón, S. Ledesma, C. Iemmi, and L. Neves, *Opt. Lett.* **38**, 4762 (2013).

[4] C. Reimer, M. Kues, P. Roztocki, B. Wetzel, F. Grazioso, B. E. Little, S. T. Chu, T. Johnston, Y. Bromberg, L. Caspani, D. J. Moss, and R. Morandotti, *Science* **351**, 1176 (2016).

[5] J. Yin, Y. Cao, Y.-H. Li, S.-K. Liao, L. Zhang, J.-G. Ren, W.-Q. Cai, W.-Y. Liu, B. Li, H. Dai, G.-B. Li, Q.-M. Lu, Y.-H. Gong, Y. Xu, S.-L. Li, F.-Z. Li, Y.-Y. Yin, Z.-Q. Jiang, M. Li, J.-J. Jia, G. Ren, D. He, Y.-L. Zhou, X.-X. Zhang, N. Wang, X. Chang, Z.-C. Zhu, N.-L. Liu, Y.-A. Chen, C.-Y. Lu, R. Shu, C.-Z. Peng, J.-Y. Wang, and J.-W. Pan, *Science* **356**, 1140 (2017).

- [6] C. J. Pugh, S. Kaiser, J.-P. Bourgoin, J. Jin, N. Sultana, S. Agne, E. Anisimova, V. Makarov, E. Choi, B. L. Higgins, and T. Jennewein, *Quantum Sci. Technol.* **2**, 024009 (2017).
- [7] S.-K. Liao, W.-Q. Cai, J. Handsteiner, B. Liu, J. Yin, L. Zhang, D. Rauch, M. Fink, J.-G. Ren, W.-Y. Liu, Y. Li, Q. Shen, Y. Cao, F.-Z. Li, J.-F. Wang, Y.-M. Huang, L. Deng, T. Xi, L. Ma, T. Hu, L. Li, N.-L. Liu, F. Koidl, P. Wang, Y.-A. Chen, X.-B. Wang, M. Steindorfer, G. Kirchner, C.-Y. Lu, R. Shu, R. Ursin, T. Scheidl, C.-Z. Peng, J.-Y. Wang, A. Zeilinger, and J.-W. Pan, *Phys. Rev. Lett.* **120**, 030501 (2018).
- [8] N. Gisin, G. Ribordy, W. Tittel, and H. Zbinden, *Rev. Mod. Phys.* **74**, 145 (2002).
- [9] K. Banaszek, A. Dragan, W. Wasilewski, and C. Radzewicz, *Phys. Rev. Lett.* **92**, 257901 (2004).
- [10] K. Sedziak, M. Lasota, and P. Kolenderski, *Optica* **4**, 84 (2017).
- [11] M. Lasota and P. Kolenderski, *Phys. Rev. A* **98**, 062310 (2018).
- [12] J. D. Franson, *Phys. Rev. Lett.* **62**, 2205 (1989).
- [13] D. Stucki, N. Brunner, N. Gisin, V. Scarani, and H. Zbinden, *Appl Phys Lett* **87**, 194108 (2005).
- [14] J. M. Donohue, M. Agnew, J. Lavoie, and K. J. Resch, *Phys. Rev. Lett.* **111**, 153602 (2013).
- [15] P. C. Humphreys, B. J. Metcalf, J. B. Spring, M. Moore, X.-M. Jin, M. Barbieri, W. S. Kolthammer, and I. A. Walmsley, *Phys. Rev. Lett.* **111**, 150501 (2013).
- [16] L. Neves, G. Lima, E. J. S. Fonseca, L. Davidovich, and S. Pádua, *Phys. Rev. A* **76**, 032314 (2007).
- [17] A. Divochiy, M. Misiaszek, Y. Vakhtomin, P. Morozov, K. Smirnov, P. Zolotov, and P. Kolenderski, *Opt. Lett.* **43**, 6085 (2018).
- [18] V. Shcheslavskiy, P. Morozov, A. Divochiy, Y. Vakhtomin, K. Smirnov, and W. Becker, *Rev. Sci. Instrum.* **87**, 053117 (2016).
- [19] B. A. Korzh, Q.-Y. Zhao, S. Frasca, J. P. Allmaras, T. M. Autry, E. A. Bersin, M. Colangelo, G. M. Crouch, A. E. Dane, T. Gerrits, F. Marsili, G. Moody, E. Ramirez, J. D. Rezac, M. J. Stevens, E. E. Wollman, D. Zhu, P. D. Hale, K. L. Silverman, R. P. Mirin, S. W. Nam, M. D. Shaw, and K. K. Berggren, 1804.06839v1.
- [20] E. Majorana, *Nuovo Cimento* **9**, 43 (1932).
- [21] P. Kolenderski, *OSID* **17**, 107 (2010).
- [22] Z. Hradil, *Phys. Rev. A* **55**, R1561 (1997).
- [23] K. Banaszek, G. M. D'Ariano, M. G. A. Paris, and M. F. Sacchi, *Phys. Rev. A* **61**, 010304 (1999).
- [24] T. Opatrny, D.-G. Welsch, and W. Vogel, *Phys. Rev. A* **56**, 1788 (1997).
- [25] D. F. V. James, P. G. Kwiat, W. J. Munro, and A. G. White, *Phys. Rev. A* **64**, 052312 (2001).
- [26] R. Jozsa, *J. Mod. Opt.* **41**, 2315 (1994).